



26

27

Abstract

28 Calcified macroalgae are critical components of marine ecosystems worldwide, but
29 face considerable threat both from climate change (increasing water temperatures) and
30 ocean acidification (decreasing ocean pH and carbonate saturation). It is thus
31 fundamental to constrain the relationships between key abiotic stressors and the
32 physiological processes that govern coralline algal growth and survival. Here we
33 characterize the complex relationships between the abiotic environment of rock pool
34 habitats, and the physiology of the geniculate red coralline alga, *Corallina officinalis*
35 (Corallinales, Rhodophyta). Paired assessment of irradiance, water temperature and
36 carbonate chemistry, with *C. officinalis* net production (*NP*), respiration (*R*) and net
37 calcification (*NG*) was performed in a south-west UK field site, at multiple temporal
38 scales (seasonal, diurnal and tidal). Strong seasonality was observed in *NP* and night-
39 time *R*, with a P_{max} of $22.35 \mu\text{mol DIC gDW}^{-1} \text{h}^{-1}$, E_k of $300 \mu\text{mol photons m}^{-2} \text{s}^{-1}$ and
40 *R* of $3.29 \mu\text{mol DIC gDW}^{-1} \text{h}^{-1}$ determined across the complete annual cycle. *NP*
41 showed a significant exponential relationship with irradiance ($R^2 = 0.67$), although was
42 temperature dependent given ambient irradiance $> E_k$ for the majority of the annual
43 cycle. Over tidal emersion periods, dynamics in *NP* highlighted the ability of *C.*
44 *officinalis* to acquire inorganic carbon despite significant fluctuations in carbonate
45 chemistry. Across all data, *NG* was highly predictable ($R^2 = 0.80$) by irradiance, water
46 temperature and carbonate chemistry, providing a NG_{max} of $3.94 \mu\text{mol CaCO}_3 \text{gDW}^{-1}$
47 h^{-1} , and E_k of $113 \mu\text{mol photons m}^{-2} \text{s}^{-1}$. Light-*NG* showed strong seasonality and
48 significant coupling to *NP* ($R^2 = 0.65$), as opposed to rock pool water carbonate
49 saturation. In contrast, the direction of dark-*NG* (dissolution vs. precipitation) was
50 strongly related to carbonate saturation, mimicking abiotic precipitation dynamics.



51 Data demonstrated that *C. officinalis* is adapted to both long-term (seasonal) and short-
52 term (tidal) variability in environmental stressors, although the balance between
53 metabolic processes and the external environment may be significantly impacted by
54 future climate change.

55

56 **1. Introduction**

57 Calcified macroalgae are critical components of marine ecosystems from polar to
58 tropical regions (Littler et al., 1985, McCoy and Kamenos, 2015), constituting one of
59 the most important structural elements in many coastal zones (van der Heijden and
60 Kamenos, 2015). In shallow temperate areas, heavily calcified ‘coralline’ red
61 macroalgae (Corallinales, Rhodophyta) act as autogenic ecosystem engineers
62 (Johansen, 1981; Jones et al., 1994; Nelson, 2009), providing habitat for numerous
63 small invertebrates, shelter from the stresses of intertidal life via their physical
64 structure, and surfaces for the settlement of epifauna and microalgal epiphytes (Nelson,
65 2009; Perkins et al., 2016). Temperate corallines are also of significant importance in
66 the carbon and carbonate cycles of shallow coastal ecosystems, due to their relatively
67 high productivity and calcium carbonate precipitation and dissolution (Martin and
68 Gattuso, 2009; van der Heijden and Kamenos, 2015).

69

70 Species of the geniculate (jointed) coralline genus *Corallina* form extensive turfs across
71 large areas of NE Atlantic intertidal regions, providing substratum, habitat and refugia
72 for a number of important organisms (Coull and Wells, 1983; Kelaher, 2002; 2003;
73 Hofmann et al., 2012a; Brodie et al., 2016; Perkins et al., 2016). Within rock pool
74 habitats, *Corallina* must maintain productivity and growth under the influence of a
75 myriad of highly variable stressors, including irradiance, water temperature and



76 carbonate chemistry, which fluctuate on seasonal, diurnal and tidal time scales
77 (Egilsdottir et al., 2013; Williamson et al., 2014a). During summer, high irradiance,
78 water temperature, pH and carbonate saturation (ΩCO_3^{2-}) dominate, whilst winter is
79 associated with limiting irradiance and temperature, and decreased water pH (i.e.
80 increased acidity) and ΩCO_3^{2-} (Ganning, 1971; Morris and Taylor, 1983; Williamson
81 et al., 2014a). Across daytime tidal emersion periods, rock pool water temperatures
82 generally increase and community photosynthetic activity serves to strip CO_2 and
83 HCO_3^- from the water, with concomitant increases in pH and ΩCO_3^{2-} (Williamson et
84 al., 2014a). In contrast, night-time emersion is dominated by respiration processes
85 within rock pools, with CO_2 production driving down water pH and ΩCO_3^{2-} (Morris
86 and Taylor, 1983). In order to sustain their dominance of temperate coastlines,
87 *Corallina* must balance this environmental variability with their requirements for key
88 physiological processes, including photosynthesis, respiration and calcification.

89

90 The interactions between *Corallina* physiology and environmental variability is likely
91 to be significantly impacted by on-going climate change (increasing temperatures) and
92 ocean acidification (decreasing pH and ΩCO_3^{2-}). It is therefore critical to constrain
93 *Corallina* ecophysiology under current environmental conditions to aid projections
94 under future climate scenarios (Nelson, 2009; Koch et al., 2013; Brodie et al., 2014;
95 Hofmann and Bischof, 2014). It is also important to understand the present-day role of
96 these dominant community members in coastal carbon cycles and how this may change
97 into the future (van der Heijden and Kamenos, 2015).

98

99 This study focuses on *Corallina officinalis*, a species that dominates North Atlantic
100 turfing assemblages (Williamson et al., 2015) and has been the focus of recent studies



101 aiming to understand coralline algal physiology and future fate (Hofmann et al.,
102 2012a,b; Williamson et al., 2014a,b; Williamson et al., 2015; Perkins et al., 2016).
103 Whilst the skeletal mineralogy (Williamson et al., 2014b), photophysiology
104 (Williamson et al., 2014a; Perkins et al., 2016), and phylogenetics of *C. officinalis*
105 (Williamson et al., 2015) have been examined, information on *in-situ* physiology in
106 relation to key environmental stressors is currently lacking. We therefore performed the
107 first high-resolution *in-situ* assessment of *C. officinalis* physiology (production,
108 respiration and calcification) in relation to key environment stressors (irradiance,
109 temperature and carbonate chemistry) over both daytime and night-time tidal emersion
110 periods, across multiple seasons. By characterizing the influence of abiotic stressors on
111 key physiological processes, this study significantly advances efforts to understand the
112 ecology and fate of coralline algae in a changing world.

113

114 2. Methods

115 This study was conducted at Combe Martin (CM), north Devon, UK (51°12'13N
116 4°2'19W, Fig. 1), a north-west facing rocky intertidal site, positioned within a sheltered
117 bay. *Corallina officinalis* dominates intertidal rock pools at CM, including large (ca. 40
118 m³, 0.5 m depth) upper shore (Chart Datum + 5.5 m) rock pools created by a man-made
119 walkway (Fig. 1b and 1c).

120

121 To assess *C. officinalis* net production, respiration and calcification, incubation
122 experiments were performed at CM during daytime tidal emersion in December 2013,
123 and March, July and September 2014, and night-time tidal emersion during the latter
124 three sampling months (sampling dates and tidal timings are presented in Table 1). Two
125 sets of approximately 1 h timed incubations were performed per emersion period, at



126 both the start (initiated within 30 mins of tidal emersion) and end (over the final 1.5 h)
127 of emersion. Irradiance and rock pool water salinity, temperature and carbonate
128 chemistry were monitored in parallel throughout.

129

130 **2.1. Physiology incubations**

131 Net production (*NP*) and respiration (*R*) (DIC flux, $\mu\text{mol g dry weight (DW)}^{-1} \text{h}^{-1}$), and
132 net light and dark calcification rates (*NG*) ($\mu\text{mol CaCO}_3 \text{gDW}^{-1} \text{h}^{-1}$) were determined
133 using closed chamber incubations. Ten discrete *C. officinalis* fronds were collected
134 randomly from upper shore CM rock pools and placed individually into 0.5 l clear glass
135 chambers filled with rock pool water. Final dry weight of incubated *C. officinalis*
136 averaged 4.0 ± 0.15 g across incubations. Two additional chambers were filled only
137 with rock pool water to serve as controls for non-*Corallina* biological activity. At the
138 beginning of incubations, five 100 ml initial rock pool water samples were collected for
139 pH and total alkalinity (TA) determination (see below), and poisoned with saturated
140 mercuric chloride solution to prevent biological activity. Incubation chambers were
141 then sealed, and six chambers (5 *Corallina*, 1 control) positioned in an upper shore rock
142 pool to maintain ambient irradiance and temperature conditions. The remaining six
143 chambers (5 *Corallina*, 1 control) were placed in opaque bags to create dark conditions
144 during daytime incubations (or shield from moonlight during night-time) and placed
145 within the same rock pool to maintain ambient temperature. After incubating for ca. 1
146 h, chambers were removed from the rock pool and a final 100 ml water sample was
147 collected from each chamber for pH and TA measurements. In parallel to all
148 incubations, ambient irradiance (PAR $\mu\text{mol photons m}^{-2} \text{s}^{-1}$), rock pool water
149 temperature ($^{\circ}\text{C}$), and salinity (S), were monitored every 30 min using a 2-pi LI-COR
150 cosine-corrected quantum sensor positioned ca. 5 cm above the surface of the rock pool



151 (15 s average irradiance measurements were taken using an in-built function of the
152 sensor), a digital thermometer, and a hand-held refractometer, respectively. Cumulative
153 photodose (PAR, mol photons m⁻²) was calculated from irradiance measurements by
154 integrating PAR over time from the start of tidal emersion of rock pools. Following
155 incubations, *C. officinalis* fronds were collected from incubation chambers for
156 weighing after drying at 100°C for 24 h.

157

158 The pH (total scale) of water samples was measured immediately using a Mettler
159 Toledo Inlab-expertpro pH probe calibrated using Tris-buffers (pH 4, 7, and 10)
160 prepared in artificial seawater. TA of water samples was measured by the
161 potentiometric method using Gran titration with a Mettler Toledo DL50 Graphix
162 automatic titrator. Reference material measurements of Na₂CO₃ standards (0.5 and 1
163 mmol kg⁻¹) prepared in 0.6 mol kg⁻¹ NaCl background medium were used to correct
164 sample measurement for accuracy. The relative error of TA measurements was 4.6 ±
165 0.24 %, with a relative standard deviation of 3.35 ± 1.5 %. pH, TA, water temperature
166 and salinity were subsequently input into CO2SYS v2.1 (Pierrot et al., 2016) to
167 determine all carbonate chemistry parameters (DIC, *p*CO₂, HCO₃⁻, CO₃²⁻ and the
168 saturation states of aragonite [Ω_{arg}] and calcite [Ω_{cal}]), allowing both calculation of *C.*
169 *officinalis* NP/R (Δ DIC) and NG (Δ TA) during incubations, and the monitoring of
170 ambient rock pool water carbonate chemistry. CO2SYS was run using the constants of
171 Mehrbach et al. (1973) refitted by Dickson and Millero (1987). The carbonate
172 chemistry of rock pool water was represented by initial water samples (n = 5) collected
173 at the beginning of each incubation experiment, providing an assessment of water
174 chemistry at both the start and end of tidal emersion periods, matching productivity
175 analyses. *C. officinalis* NP (assessed from daytime light treatment incubations) and *R*



176 (assessed from daytime dark treatment and all night-time incubations) were calculated
 177 from the difference between initial and final incubation DIC concentrations, as:

178

$$179 \quad NP \text{ or } R_{DAY/NIGHT} = \left(\frac{\Delta DIC}{dw \Delta t} v \right) - NG$$

180

181 where NP and $R_{DAY/NIGHT}$ are net production and respiration during the day or night,
 182 respectively ($\mu\text{mol DIC gDW}^{-1} \text{ h}^{-1}$); ΔDIC is the change in dissolved inorganic carbon
 183 concentration during the incubation ($\mu\text{mol DIC kg}^{-1}$ seawater); v is the incubation
 184 chamber volume (l); dw is the dry weight of *C. officinalis* incubated (g); Δt is the
 185 incubation time (h); and NG is the net calcification rate ($\mu\text{mol CaCO}_3 \text{ gDW}^{-1} \text{ h}^{-1}$). NG
 186 was estimated using the alkalinity anomaly technique (Smith and Key, 1975; Chisholm
 187 and Gattuso, 1991), whereby TA decreases by 2 equivalents for each mol of CaCO_3
 188 precipitated. Light calcification (assessed from daytime light treatment incubations)
 189 and dark calcification (assessed from daytime dark and all night-time incubations) were
 190 thus calculated as:

$$191 \quad NG_{DAY} \text{ (or } NG_{NIGHT})_{-LIGHT/DARK} = \frac{\Delta TA v}{2(dw \Delta t)}$$

192

193 where $NG_{DAY-LIGHT/DARK}$ and $NG_{NIGHT-LIGHT/DARK}$ are net calcification during daytime or
 194 night-time tidal emersion periods, determined from light or dark treatment incubations
 195 ($\mu\text{mol CaCO}_3 \text{ gDW}^{-1} \text{ h}^{-1}$); ΔTA is the change in total alkalinity during the incubation
 196 ($\mu\text{mol kg}^{-1}$ seawater); v is the incubation chamber volume (l); dw is the dry weight of
 197 *C. officinalis* incubated (g); and Δt is the incubation time (h).

198

199 **2.2. Data analysis**



200 All statistical analyses and plotting of data were performed using R v.3.0.2 (R Core
201 Team, 2014). Prior to all analyses, normality of data was tested using the Shapiro-Wilk
202 test and examination of frequency histograms. If data were not normally distributed,
203 Box-Cox power transformation was applied using the boxcox function of the MASS
204 package (Venables and Ripley, 2002), and normality re-checked. Following the
205 application of models to data, model assumptions were checked by examination of
206 model criticism plots. Whilst sampling for determination of NP , R and NG was
207 performed in the same rock pools over a number of dates at each site, measurements
208 were performed on different individuals during each sampling date and thus repeated
209 measures analysis of variance (ANOVA) was not utilized during the present study.

210

211 *Abiotic Environment:* Differences in irradiance and rock pool water temperature
212 between sampling months and tidal emersion periods were examined using 2-way
213 ANOVA with interaction. Post hoc Tukey honest significant differences analysis was
214 performed on all significant ANOVA results. To facilitate comparison of rock pool
215 water carbonate chemistry between months and tidal emersion periods, all variables
216 were summarized using principal components analysis (PCA) with scaled variables,
217 allowing for transformation of the highly correlated carbonate chemistry variables into
218 uncorrelated PCs for comparison between independent variables (month and tide).
219 Differences in carbonate chemistry were thus examined by ANOVA analysis of
220 principal component one (PC1) separately for daytime and night-time data, as above.
221 Least squares multiple linear regression was used to examine relationships between
222 daytime PC1 and irradiance (analysed separately as both irradiance measured and
223 calculated cumulative photodose) and rock pool water temperature. The relative
224 importance of predictor variables was calculated using the relaimpo package with type



225 ‘lmg’ (Grömping, 2006). Least squares linear regression was used to examine
226 relationships between night-time PC1 and rock pool water temperature.

227

228 *Net production, respiration and calcification:* NP , $R_{DAY/NIGHT}$ and NG rates were
229 analyzed separately for daytime and night-time data using 3-way ANOVA with the
230 factors month, tide and light-treatment, with all interactions. All *C. officinalis* NP/R and
231 NG data were plotted as an exponential function $P-E$ of ambient irradiance E (μmol
232 photons $\text{m}^{-2} \text{s}^{-1}$), as:

233

$$234 \quad NP/R (NG) = P_{max}(1 - e^{-E/E_k}) + c$$

235

236 where P_{max} is the rate of maximum net production (or calcification) ($\mu\text{mol DIC gDW}^{-1}$
237 h^{-1} , or $\mu\text{mol CaCO}_3 \text{ gDW}^{-1} \text{ h}^{-1}$); E_k is the minimum saturating irradiance ($\mu\text{mol m}^{-2} \text{s}^{-1}$);
238 and c is the dark respiration rate (or calcification rate) ($\mu\text{mol DIC/CaCO}_3 \text{ gDW}^{-1} \text{ h}^{-1}$).

239 To examine relationships between NP , R and NG with water temperature and carbonate
240 chemistry ($\text{PC1}_{\text{day/night}}$), temperature and PC1 were added individually into the above
241 model as linear terms, in addition to construction of a ‘global model’ containing
242 irradiance as an exponential function, and both water temperature and PC1 as linear
243 terms. The goodness-of-fit of the respective models was compared using estimated R^2
244 and Akaike Information Criterion (AIC), and ANOVA comparisons were performed to
245 test the significance of the inclusion of respective terms into each model. The
246 relationship between *C. officinalis* NG and NP/R was modeled using non-linear
247 regression as detailed above.

248

249 **3. Results**



250 3.1. Abiotic environment

251 Irradiance varied between all sampling months ($F_{3,32} = 193.385$, $P < 0.0001$), being
252 maximal in July and minimal in December (Fig. 2), with significant change in
253 irradiance over tidal emersion only apparent in July ($F_{1,32} = 8.114$, $P < 0.01$, TukeyHSD
254 $P < 0.05$). Warmest daytime rock pool water temperatures were observed in July, with
255 the coldest in March, and a significant difference apparent between all sampling months
256 ($F_{3,32} = 760.94$, $P < 0.0001$) (Fig. 2). Water temperature significantly increased over
257 daytime tidal emersion during July and September ($F_{1,32} = 97.48$, $P < 0.0001$,
258 TukeyHSD $P < 0.05$ in both cases), whereas no change occurred in December or March,
259 as supported by significant interaction between month and tide ($F_{3,32} = 37.01$, $P <$
260 0.0001). Night-time rock pool water temperatures were greatest in September and
261 lowest in March, with a significant difference between all sampling months ($F_{2,13} =$
262 168.534 , $P < 0.0001$). Over night-time tidal emersion, a significant decrease in water
263 temperature was apparent during July (15.6 ± 0.16 to $14.7 \pm 0.14^\circ\text{C}$) and September
264 (16.8 ± 0.45 to $15.7 \pm 0.15^\circ\text{C}$) ($F_{1,13} = 20.049$, $P < 0.01$, TukeyHSD $P < 0.05$ in all
265 cases).

266

267 Changes in rock pool water carbonate chemistry were observed over daytime and night-
268 time tidal emersion periods during each sampling month (Supplementary Figures 1 &
269 2). Over daytime emersion, $p\text{CO}_2$ and HCO_3^- decreased, with concomitant increases in
270 pH, CO_3^{2-} , Ω_{arg} and Ω_{cal} . From the start to end of night-time emersion, the opposite
271 trends were observed, with increases in $p\text{CO}_2$ and HCO_3^- paralleled by decreases in pH
272 and $\Omega_{\text{CO}_3^{2-}}$. Principal components analysis (PCA) served to summarize daytime and
273 night-time carbonate chemistry parameters for subsequent analyses (Table 2 & Fig. 3),
274 with PC1_{day} and $\text{PC1}_{\text{night}}$ describing 84 % and 83 % of the variance in carbonate



275 chemistry observed over seasonal and tidal time-scales, respectively. For all subsequent
276 analyses, $PC1_{\text{day}}$ and $PC1_{\text{night}}$ were taken as representative of carbonate chemistry
277 dynamics.

278

279 $PC1_{\text{day}}$ and $PC1_{\text{night}}$ were significantly different between sampling months ($F_{3,67} =$
280 27.528 and $F_{2,47} = 39.73$, respectively, $P < 0.0001$ in both cases, Fig. 4), with higher
281 $PC1_{\text{day}}$ observed in July and September in comparison to December and March, and
282 significantly different $PC1_{\text{night}}$ observed between all night-time sampling months
283 (March, July and September; TukeyHSD, $P < 0.05$ in all cases). $PC1_{\text{day}}$ significantly
284 increased over daytime tidal emersion, representing decreased DIC, $p\text{CO}_2$ and HCO_3^- ,
285 and increased pH and ΩCO_3^{2-} parameters, during all sampling months but December
286 ($F_{1,67} = 1.912$, $P < 0.0001$, TukeyHSD $P < 0.05$ in all cases). Over night-time tidal
287 emersion the opposite trends were observed, with significant decrease in $PC1_{\text{night}}$
288 apparent during every sampling month, representing increased DIC, $p\text{CO}_2$ and HCO_3^-
289 and consequent decreases in pH and ΩCO_3^{2-} ($F_{1,47} = 810.90$, $P < 0.0001$, TukeyHSD P
290 < 0.05 in all cases). The magnitude of change in rock pool water carbonate chemistry
291 over night-time tidal emersion increased from March to September, as evidenced by
292 significant interaction between month and tide ($F_{2,47} = 73.31$, $P < 0.0001$).

293

294 Least squares multiple linear regression (Table 3) revealed significant relationships
295 between $PC1_{\text{day}}$, irradiance (28% relative importance) and water temperature (71%
296 relative importance) ($R^2 = 0.63$, $P < 0.0001$) (Table 3), and between $PC1_{\text{day}}$, calculated
297 cumulative photodose (58% relative importance) and water temperature (41% relative
298 importance) ($R^2 = 0.69$, $P < 0.0001$). $PC1_{\text{night}}$ showed a minimal relationship to water
299 temperature ($R^2 = 0.08$, $P < 0.05$).



300

301 **3.2. Net production and respiration**

302 *Corallina officinalis* demonstrated maximal *NP* (negative DIC flux) in July (start of
303 emersion = $25.80 \pm 0.94 \mu\text{mol DIC gDW}^{-1} \text{ h}^{-1}$), with lowest values recorded during
304 December and March (end of March emersion = $1.56 \pm 0.74 \mu\text{mol DIC gDW}^{-1} \text{ h}^{-1}$)
305 ($F_{3,69} = 6.838, P < 0.001$) (Fig. 5). In contrast, no significant difference in *C. officinalis*
306 R_{DAY} was observed between sampling months (Fig. 5a). Whilst significant changes in
307 NP and R_{DAY} were recorded in relation to the factor tide ($F_{1,69} = 8.684, P < 0.01$), post-
308 hoc TukeyHSD did not recover significant differences in either parameter between the
309 start and end of tidal emersion, within any sampling month. Over night-time tidal
310 emersion, no significant difference was apparent in R_{NIGHT} between light treatment or
311 the start and end of tidal emersion periods, and thus data are pooled for presentation
312 (Fig. 6a). Across sampling months, a significant increase in *C. officinalis* R_{NIGHT} was
313 apparent from March to July and September ($F_{2,52} = 22.170, P < 0.0001$), with ca. 4.5-
314 fold greater R_{NIGHT} observed during September as compared to March.

315

316 Across all data, NP showed a significant relationship with irradiance ($R^2 = 0.67, P <$
317 0.0001 for all parameters, $AIC = 885.64$), giving a P_{max} of $22.35 \mu\text{mol DIC gDW}^{-1} \text{ h}^{-1}$,
318 E_k of $301 \mu\text{mol photons m}^{-2} \text{ s}^{-1}$ and estimated overall respiration rate of $3.29 \mu\text{mol DIC}$
319 $\text{gDW}^{-1} \text{ h}^{-1}$ (Fig. 7a, Table 4). Addition of water temperature and carbonate chemistry
320 (both individually and together) into the model did not significantly improve the
321 goodness-of-fit (Table 4). This may be due to correlations between irradiance and water
322 temperature ($r = 0.42, P < 0.0001$), irradiance and PC1 ($r = 0.19, P < 0.05$) and
323 temperature and PC1 ($r = 0.59, P < 0.0001$) (data not shown).

324



325 3.3. Calcification

326 *Corallina officinalis* NG_{DAY} was greatest during July and September as compared to
327 December and March ($F_{3,69} = 16.814$, $P < 0.0001$, TukeyHSD $P < 0.05$ in all cases),
328 with a significant difference between $NG_{DAY-LIGHT}$ and $NG_{DAY-DARK}$ apparent in all
329 sampling months ($F_{1,69} = 290.075$, $P < 0.0001$) (Fig. 5b). Highest $NG_{DAY-LIGHT}$ ($4.62 \pm$
330 $0.45 \mu\text{mol CaCO}_3 \text{ gDW}^{-1} \text{ h}^{-1}$) was recorded at the end of daytime tidal emersion during
331 July, with lowest $NG_{DAY-LIGHT}$ ($1.70 \pm 0.08 \mu\text{mol CaCO}_3 \text{ gDW}^{-1} \text{ h}^{-1}$) recorded at the end
332 of tidal emersion during December. Both negative (indicating CaCO_3 dissolution) and
333 positive (indicating CaCO_3 precipitation) $NG_{DAY-DARK}$ values were observed, with
334 maximal CaCO_3 dissolution in the dark ($-0.53 \pm 0.20 \mu\text{mol CaCO}_3 \text{ gDW}^{-1} \text{ h}^{-1}$) at the
335 start of March daytime tidal emersion and maximal precipitation in the dark ($2.01 \pm$
336 $0.35 \mu\text{mol CaCO}_3 \text{ gDW}^{-1} \text{ h}^{-1}$) at the end of September daytime tidal emersion (Figure
337 5b). Significant differences in NG_{DAY} observed in relation to tide ($F_{1,69} = 5.028$, $P <$
338 0.05) were confined to increases in $NG_{DAY-DARK}$ from the start to end of July and
339 September tidal emersion periods (TukeyHSD $P < 0.05$ in both cases), with significant
340 interaction between month and tide ($F_{3,69} = 5.104$, $P < 0.01$). No significant differences
341 in $NG_{DAY-LIGHT}$ were observed between the start and end of tidal emersion periods
342 despite concomitant increases in rock pool water ΩCO_3^{2-} .

343

344 During night-time tidal emersion, there was no significant difference between NG_{NIGHT-}
345 $LIGHT$ and $NG_{NIGHT-DARK}$, or between the start and end of tidal emersion within any
346 sampling month, and thus data are pooled for presentation (Fig. 6b). Whilst net CaCO_3
347 dissolution was observed during both March and September night-time tidal emersion,
348 with maximal dissolution in the latter month (monthly average of $-0.83 \pm 0.11 \mu\text{mol}$
349 $\text{CaCO}_3 \text{ gDW}^{-1} \text{ h}^{-1}$), net CaCO_3 precipitation was apparent across the duration of July



350 night-time emersion (monthly average of $0.46 \pm 0.14 \mu\text{mol CaCO}_3 \text{ gDW}^{-1} \text{ h}^{-1}$); rates
351 being significantly different between all sampling months ($F_{2,52} = 25.50$, $P < 0.0001$,
352 TukeyHSD $P < 0.05$ in all cases) (Fig. 6b).

353

354 Across all data, NG showed a significant exponential relationship with ambient
355 irradiance (estimated $R^2 = 0.76$, $P < 0.0001$ for all parameters, $AIC = 383.17$), providing
356 a NG_{max} of $4.41 \mu\text{mol CaCO}_3 \text{ gDW}^{-1} \text{ h}^{-1}$, and an E_k of $201 \mu\text{mol photons m}^{-2} \text{ s}^{-1}$ (Fig.
357 7b, Table 4). Addition of water temperature and/or carbonate chemistry (as PC1)
358 increased the goodness-of-fit (estimated R^2 and AIC) of the models to NG data (Table
359 4). The best representation of NG was provided by the ‘global model’ including
360 irradiance as exponential term, and both water temperature and carbonate chemistry as
361 linear terms (estimated $R^2 = 0.80$, $P < 0.05$ for all parameters, $AIC = 360.57$), providing
362 a NG_{max} of $3.94 \mu\text{mol CaCO}_3 \text{ gDW}^{-1} \text{ h}^{-1}$, and an E_k of $113 \mu\text{mol photons m}^{-2} \text{ s}^{-1}$ (Table
363 4). ANOVA comparison demonstrated all NG models to be significantly different to
364 one another (data not shown). Across all data, a significant relationship was also
365 identified between NG and NP/R ($R^2 = 0.65$, $P < 0.05$ for all parameters, $n = 140$) (Fig.
366 8).

367 4. Discussion

368 Through the pairing of physiological and environmental monitoring, this study has
369 constrained the regulation of key physiological processes of a coralline alga by
370 irradiance, water temperature and carbonate chemistry. It is fundamental to understand
371 the interactions of coralline algae with their environment, given the continuing
372 perturbation of key abiotic stressors by climate change and ocean acidification. The
373 knowledge presented here significantly advances our understanding of the



374 ecophysiology of *Corallina officinalis*, which will be vital when making future
375 projections for the fate of this ecosystem engineer.

376

377 **4.1. Production and respiration**

378 This study highlights significant seasonality in *C. officinalis* net production that follows
379 dynamics in irradiance, water temperature and carbonate chemistry. In marine
380 macrophytes, photosynthetic capacity is generally greatest during months when
381 irradiance and temperature are highest (Lüning, 1990; Cabello-Pasini and Alberte,
382 1997). Consistent with previous accounts for other calcifying macroalgae (e.g. Martin
383 et al., 2006; 2007; Egilsdottir et al., 2015), *C. officinalis* net production was maximal
384 during July and minimal in December, showing a significant exponential relationship
385 with irradiance ($R^2 = 0.67$). Whilst inclusion of water temperature and carbonate
386 chemistry into models did not improve predictive ability, co-variance between
387 predictors may have hindered interpretation of their influence. At saturating levels of
388 irradiance, the enzymatic reactions that limit photosynthesis are temperature dependent
389 (Lüning, 1990). The light-saturation coefficient (E_k) determined by the present study
390 (ca. 300 $\mu\text{mol photons m}^{-2} \text{s}^{-1}$ ambient irradiance) highlighted that *C. officinalis*
391 photosynthesis was light-saturated for the majority of the annual cycle; ambient
392 irradiance $> E_k$ was recorded in every sampling month other than December, consistent
393 with the findings of Williamson et al. (2014a). Thus maximal rates of *C. officinalis*
394 production were likely temperature-dependent, as is known for other intertidal
395 macroalgae (Kanwisher, 1966).

396

397 Strong seasonality was also identified in *C. officinalis* dark respiration determined
398 during night-time incubations, in line with accounts for other coralline algae (e.g.



399 Martin et al., 2006; Egilsdottir et al., 2015). The ca. 4.5-fold increase observed in night-
400 time respiration from March to September is within the range reported for the maerl-
401 forming species, *Lithothamnion coralloides*, which demonstrated a 3-fold increase in
402 respiration during summer months (Martin et al., 2006), and the closely related
403 geniculate species, *Ellisolandia elongata*, which demonstrated a 10-fold summer
404 increase in respiration (Egilsdottir et al., 2015). Whilst night-time respiration rates
405 determined here for *C. officinalis* (ca 1 – 4.5 $\mu\text{mol DIC gDW}^{-1} \text{h}^{-1}$) fall within the lower
406 end of the range reported for *E. elongata* from similar habitats (ca. 0.4 - 17 $\mu\text{mol CO}_2$
407 $\text{gDW}^{-1} \text{h}^{-1}$), Egilsdottir et al. (2015) note that their high summer rates were likely driven
408 by high water temperatures during summer measurements (23°C as compared to 16°C
409 during the present study).

410

411 Consistent with observations made in *E. elongata* dominated habitats (Bensoussan and
412 Gattuso, 2007), *C. officinalis* demonstrated increased rates of daytime respiration as
413 compared to night-time, with 6-fold greater daytime rates during March, and 1.1-times
414 greater rates during July and September. Previously, Bensoussan and Gattuso (2007)
415 observed large variations in winter respiratory activity under both daylight and dark
416 conditions in assemblages dominated by *E. elongata*, with significantly higher
417 respiration during the afternoon and first part of the night. Such diurnal variations are
418 reflected by our findings, with maximal daytime respiration decreasing to lower levels
419 across night-time emersion. Our data further demonstrated that seasonality in
420 respiration was better reflected by night-time incubations, whereas no seasonal patterns
421 were apparent in daytime rates. This is likely due to the influence of residual biological
422 activity after passage from light to dark conditions, given differences in the photo-
423 history of day and night incubated *C. officinalis*. Daytime samples were collected from



424 100% ambient irradiance and immediately transferred to complete darkness, whereas
425 night-time samples had been in darkness for a number of hours prior to incubations.
426 Future assessments may benefit from use of, for example, the Kok method for
427 determination of light respiration rates, as applied by Zou et al. (2011) to several
428 macroalgal species.

429

430 Differences between light and dark respiration rates have direct consequences for the
431 conventional calculation of gross production ($GP = \text{net production} + \text{respiration}$)
432 (Bensoussan and Gattuso, 2007), although estimates can be made for *C. officinalis*
433 using our data. Net production recorded at the start of tidal emersion ranged seasonally
434 from ca. 11 (December) to 26 (July) $\mu\text{mol DIC gDW}^{-1} \text{h}^{-1}$. Assuming our lower,
435 seasonally variable night-time rates of respiration to be representative, *C. officinalis* GP
436 is estimated as ranging 15.9 (March) to 27.7 (July) $\mu\text{mol DIC gDW}^{-1} \text{h}^{-1}$; though
437 December data are omitted due to the absence of night-time incubations. Similarly,
438 correcting net production with daytime respiration rates reveals a GP range of 16.7
439 (December) to 27.8 (July) $\mu\text{mol DIC gDW}^{-1} \text{h}^{-1}$ for *C. officinalis*. These estimates are
440 highly comparable to GP reported for *E. elongata* from NW France during winter (11.8
441 $\pm 1.6 \mu\text{mol C gDW}^{-1} \text{h}^{-1}$) and summer ($22.5 \pm 1.9 \mu\text{mol C gDW}^{-1} \text{h}^{-1}$) (Egilsdottir et al.,
442 2015), and serve to highlight the high productivity of geniculate corallines in
443 comparison to other calcified algal groups. For example, Martin et al. (2006) reported
444 a seasonal range of 0.68 to 1.48 $\mu\text{mol C gDW}^{-1} \text{h}^{-1}$ for the maerl forming *Lithothamnion*
445 *coralloides* off NW France. Currently, the contribution of coralline algae to global
446 carbon cycles is not well constrained, particularly that of geniculate turfing species (El
447 Haikali et al., 2004; Van der Heijden and Kamenos, 2015). Given their comparatively
448 high production identified here, our data indicate that geniculate corallines likely play



449 a significant role in coastal carbon cycling, despite their presumably reduced overall
450 benthic coverage as compared to maerl-forming or crustose coralline algal species.
451 Inclusion of geniculate corallines into future estimates of coastal carbon cycles is
452 therefore essential.

453

454 Over tidal emersion periods, patterns in *C. officinalis* production demonstrate the
455 inorganic carbon (*C_i*) acquisition ability of this calcified alga over a range of CO₂ and
456 HCO₃⁻ concentrations, however findings indicate potential vulnerability to periods of
457 low irradiance e.g. winter. Maintenance of net production over July and September
458 daytime tidal emersion, despite decreases in rock pool *p*CO₂ of 84% and 39%,
459 respectively, highlight the ability of *C. officinalis* to effectively utilize both CO₂ and
460 HCO₃⁻ as substrates for photosynthesis, as previously noted (Cornwall et al., 2012).

461 This allows access to the relatively high HCO₃⁻ concentrations in seawater when CO₂
462 diffusion is limiting (Koch et al., 2013). During December and March, however, when
463 overall minimal irradiance prevailed, a decrease in *C. officinalis* net production was
464 observed. Estimation of *GP/R* ratios for these emersion periods (using daytime
465 respiration data) revealed decreases from 3.45 to 1.9 over December-, and 3.93 to 1.2
466 over March- daytime emersion. Thus decreases in net production were driven by
467 decreases in photosynthesis relative to respiration, which approached unity by the end
468 of emersion in winter months. This reflects ecosystem wide *GP/R* ratios for
469 assemblages dominated by *E. elongata* in the NW Mediterranean, which remained close
470 to 1 (1.1 ± 0.1) over 24 h periods during winter (Bensoussan and Gattuso, 2007).

471 Although water temperature, nor irradiance, showed significant change over December
472 or March tidal emersion, reductions in photosynthesis may have been driven by
473 inorganic carbon limitation due to seasonal minima in irradiance. Under low light



474 conditions, the ability to utilize HCO_3^- can be energetically limited, increasing reliance
475 on CO_2 diffusion (Koch et al., 2013). *C. officinalis* photosynthesis may thus have been
476 sensitive to the relatively small decrease in rock pool $p\text{CO}_2$ (ca. 30%) that occurred
477 over December and March emersion periods.

478

479 **4.2. Calcification**

480 This study demonstrates that *C. officinalis* calcification is highly influenced by seasonal
481 and diurnal variability in other metabolic processes (photosynthesis and respiration), in
482 addition to the external carbonate chemistry environment. Across the entire annual
483 cycle, *C. officinalis* calcification was highly predictable ($R^2 = 0.80$) by irradiance, water
484 temperature and carbonate chemistry, providing a calculated NG_{max} of $3.94 \mu\text{mol}$
485 $\text{CaCO}_3 \text{ gDW}^{-1} \text{ h}^{-1}$ and an E_k of $113.45 \mu\text{mol photons m}^{-2} \text{ s}^{-1}$. Irradiance was the greatest
486 predictor of calcification (accounting for 76% of variability), reflecting photosynthetic
487 enhancement of CaCO_3 precipitation (see below), although by contrasting light and
488 dark calcification dynamics, the variable influences of physiology and external
489 environment have been determined.

490

491 Light-enhanced calcification, i.e. CaCO_3 precipitation, was observed across the entire
492 seasonal cycle, with maximal light-calcification rates during July and September in
493 comparison to December and March. The seasonal range of net light-calcification was
494 significantly higher than reported for the maerl species *L. corallioides* (Martin et al.,
495 2006), comparable to *E. elongata* from NW France (Egilsdottir et al., 2015), and lower
496 than reported for *E. elongata* from the Mediterranean (El Haïkali et al., 2004). Light-
497 enhanced calcification is typical for calcifying macroalgae, and is a product of light-
498 dependent increase in carbonate saturation (ΩCO_3^{2-}) at the sites of calcification, due to



499 photosynthetic activity (Littler, 1976; Koch et al., 2013). In the Corallinales,
500 calcification takes place in the cell wall, from which CO_2 (and potentially HCO_3^-)
501 uptake by adjacent cells for photosynthesis increases the pH, shifting the carbonate
502 equilibrium in favour of ΩCO_3^{2-} and CaCO_3 precipitation (Littler, 1976; Borowitzka,
503 1982; Koch et al., 2013). Photosynthetic enhancement of *C. officinalis* calcification
504 during the present study is strongly supported by the significant relationship identified
505 between the two processes ($R^2 = 0.65$), as was also observed by Pentecost (1978).
506 Interestingly, our data further demonstrated that internal enhancement of ΩCO_3^{2-} at the
507 site of calcification, as opposed to external ΩCO_3^{2-} , was the dominant control on light-
508 calcification rates. This was evidenced by a lack of increase in light calcification rates
509 over summer tidal emersion periods, despite significant increases in rock pool pH and
510 ΩCO_3^{2-} . With decreases in net production over daytime tidal emersion, e.g. during
511 March, minimal levels of production were sufficient to maintain increased internal
512 ΩCO_3^{2-} , permitting maintenance of calcification. This is supported by the overall lower
513 E_k determined for calcification (ca. $110 \mu\text{mol photons m}^{-2} \text{ s}^{-1}$) as compared to net
514 production (ca. $300 \mu\text{mol photons m}^{-2} \text{ s}^{-1}$).

515

516 In contrast to light calcification, the direction of *C. officinalis* dark calcification
517 (dissolution vs. precipitation) was strongly related to rock pool water ΩCO_3^{2-} ,
518 mimicking abiotic CaCO_3 precipitation dynamics (Millero, 2007; Ries 2009). During
519 seasonal minima of ΩCO_3^{2-} , net dissolution of CaCO_3 was apparent across dark daytime
520 (December) and night-time (March) incubations, as observed during winter for *E.*
521 *elongata* (Egilsdottir et al., 2015). With increases in pH and ΩCO_3^{2-} over March, July
522 and September daytime tidal emersion, initially negative (indicating net dissolution) or
523 low positive dark calcification rates increased significantly, indicating net CaCO_3



524 precipitation at levels 40 – 46 % of light calcification. Additionally, net CaCO_3
525 precipitation was recorded across all dark daytime and night-time incubations during
526 July, coinciding with seasonal maxima in ΩCO_3^{2-} . CaCO_3 precipitation in the dark has
527 previously been documented for calcifying macroalgae (e.g. Pentecost, 1978;
528 Borowitzka, 1981; Gao et al., 1993; Lee and Carpenter, 2001; de Beer and Larkum,
529 2001; Martin et al., 2006), typically at lower rates (e.g. 10 – 40 %) than light
530 calcification (Pentecost, 1978; Borowitzka, 1981), and has been attributed to belated
531 biological activity after a passage from light to dark conditions (Pentecost, 1978; Martin
532 et al., 2006). Our findings demonstrate that dark calcification is possible over complete
533 diurnal cycles for *C. officinalis*, and can be significantly exaggerated under conditions
534 of rock pool water CO_3^{2-} -super-saturation. This mechanism can, however, be
535 overridden by enhanced respiration. At the level of the organism, respiration can
536 promote CaCO_3 dissolution via internal generation of CO_2 (Koch et al., 2013). During
537 September, when maximal night-time respiration was observed, net CaCO_3 dissolution
538 was apparent over the duration of night-time emersion, despite seasonal highs in
539 ΩCO_3^{2-} . Dissolution pressures can thus be exacerbated by high rates of respiration,
540 mitigating the positive impacts of maxima in external ΩCO_3^{2-} . This may have
541 significant ramifications for the future fate of coralline algae if increases in water
542 temperature drive corresponding increases in respiration.

543

544 **Conclusions**

545 Our findings indicate that *Corallina* species are highly tolerant to environmental stress,
546 and are well-adapted to intertidal habitats, in agreement with previous studies
547 (Williamson et al., 2014; Guenther and Martone, 2014). Photosynthesis, respiration and
548 calcification varied significantly with abiotic stressors, and strongly interacted with one



549 another to produce predominantly beneficial outcomes at the level of the organism.
550 With predicted acidification and warming of the world's oceans, the balance between
551 these processes and the external environment may be perturbed. Whilst acidification
552 may relieve putative CO₂ limitation in rock pools during low irradiance winter months,
553 increases in night-time dissolution are predicted given the strong coupling between
554 carbonate chemistry and dark calcification dynamics identified here. Similarly, whilst
555 increasing temperatures may facilitate increases in gross productivity, temperature
556 driven increases in night-time respiration could further exacerbate dark dissolution by
557 reducing carbonate saturation at the sites of calcification. *Corallina officinalis* will be
558 most vulnerable to future change during winter months, and monitoring to assess
559 impacts should be focused on such periods. This study adds to the growing
560 understanding of coralline algal physiology, and provides a baseline against which to
561 monitor future change.

562
563

Acknowledgements

564 This work was funded by the NERC grant (NE/H025677/1).

565

566

References

- 567 Bensoussasn, N. and Gattuso, J-P.: Community primary production and calcification in
568 a NW Mediterranean ecosystem dominated by calcareous macroalgae, *Mar. Ecol. Prog.*
569 *Ser.*, 334, 37–45, 2007.
570
571 Borowitzka, M.A.: Photosynthesis and calcification in the articulated coralline red
572 algae *Amphiroa anceps* and *A. foliacea*, *Mar. Biol.*, 62, 17–23, 1981.
573
574 Borowitzka, M.A.: Morphological and cytological aspects of algal calcification, *Int.*
575 *Rev. Cytol. Surv. Cell Biol.*, 74, 127–162, 1982.
576
577 Brodie, J., Williamson, C., Barker, G.L., Walker, R.H., Briscoe, A., and Yallop, M.:
578 Characterising the microbiome of *Corallina officinalis*, a dominant calcified intertidal
579 red alga, *FEMS Micro. Ecol.*, 92(8), doi: 10.1093/femsec/fiw110, 2016.
580
581



- 582
 583 Brodie, J., Williamson, C.J., Smale, D.A. et al.: The future of the north-east Atlantic
 584 benthic flora in a high CO₂ world, *Ecology and Evolution*, 4(13), 2787–2798, 2014.
 585
 586 Cabello-Pasini, A. and Alberte, R.S.: Seasonal patterns of photosynthesis and light-
 587 independent carbon fixation in marine macrophytes, *J. Phycol.*, 33, 321–329, 1997.
 588
 589 Chisholm, J.R.M. and Gattuso, J.P.: Validation of the alkalinity anomaly technique for
 590 investigating calcification and photosynthesis in coral-reef communities, *Limnol.*
 591 *Oceanogr.*, 36, 1232–1239, 1991.
 592
 593 Cornwall, C.E., Hepburn, C.D., Pritchard, D., Currie, K.I., McGraw, C.M., Hunter,
 594 K.A. and Hurd, C.L.: Carbon-use strategies in macroalgae: differential responses to
 595 lowered pH and implications for ocean acidification, *J. Phycol.*, 48, 137–144, 2012.
 596
 597 Coull, B.C. and Wells, J.B.J.: Refuges from fish predation - experiments with phytal
 598 meiofauna from the New Zealand rocky intertidal, *Ecology*, 64, 1599–1609, 1983.
 599
 600 De Beer, D. and Larkum, A.W.D.: Photosynthesis and calcification in the calcifying
 601 algae *Halimeda discoidea* studied with microsensors, *Plant Cell Environ.*, 24, 1209–
 602 1217, 2001.
 603
 604 Dickson, A.G. and Millero, F.J.: A comparison of the equilibrium constants for the
 605 dissociation of carbonic acid in seawater media. *Deep Sea Res. Part A Oceanogr. Res.*
 606 *Pap.*, 34, 1733–1743, 1987.
 607
 608 Egilsdottir, H., Olafsson, J. and Martin, S.: Photosynthesis and calcification in the
 609 articulated coralline alga *Ellisolandia elongata* (Corallinales, Rhodophyta) from
 610 intertidal rock pools, *Eur. J. Phycol.*, 51(1), 59–70, 2015.
 611
 612 Egilsdottir, H., Noisette, F., Noël, L.M.-L.J., Olafsson, J. and Martin, S.: Effects of
 613 pCO₂ on physiology and skeletal mineralogy in a tidal pool coralline alga *Corallina*
 614 *elongata*, *Mar. Biol.*, 160, 2103–2112, 2013.
 615
 616 El Haïkali, B., Bensoussan, N., Romano, J. and Bousquet, V.: Estimation of
 617 photosynthesis and calcification rates of *Corallina elongata* Ellis and Solander, 1786,
 618 by measurements of dissolved oxygen, pH and total alkalinity, *Sci. Mar.*, 68, 45–56,
 619 2004.
 620
 621 Ganning, B.: Studies on chemical, physical and biological conditions in Swedish
 622 rockpool ecosystems, *Ophelia*, 9, 51–105, 1971.
 623
 624 Gao, K., Aruga, Y., Asada, K., Ishihara, T., Akano, T. and Kiyohara, M.: Calcification
 625 in the articulated coralline alga *Corallina pilulifera*, with special reference to the effect
 626 of elevated CO₂ concentration, *Mar. Biol.*, 117, 129–132, 1993.
 627
 628 Grömping, U.: Relative Importance for linear regression in R: The Package relaimpo,
 629 *J. Stat. Softw.*, 17, 1–27, 2006.
 630



- 631 Guenther, R.J. and Martone, P.T.: Physiological performance of intertidal coralline
632 algae during a simulated tidal cycle, *J. Phycol.*, 50, 310–321, 2014.
633
- 634 Hofmann, L. and Bischof, K.: Ocean acidification effects on calcifying macroalgae,
635 *Aquat. Biol.*, 22, 261–279, 2014.
636
- 637 Hofmann, L., Straub, S. and Bischof, K.: Competition between calcifying and
638 noncalcifying temperate marine macroalgae under elevated CO₂ levels, *Mar. Ecol.*
639 *Prog. Ser.*, 464, 89–105, 2012a.
640
- 641 Hofmann, L., Yildiz, G., Hanelt, D. and Bischof, K.: Physiological responses of the
642 calcifying rhodophyte, *Corallina officinalis* (L.), to future CO₂ levels, *Mar. Biol.* 159,
643 783–792, 2012b.
644
- 645 Johansen, H.W.: *Coralline Algae: A first synthesis*. CRC Press, Boca Raton, Florida,
646 USA. p239, 1981.
647
- 648 Jones, C.G., Lawton, J.H. and Shachak, M.: Organisms as ecosystem engineers, *Oikos*,
649 69, 373–386, 1994.
650
- 651 Kanwisher, J.: Photosynthesis and respiration in some seaweeds. In: Barnes H (ed)
652 *Some Contemporary Studies in Marine Science*. George Allen and Unwin LTD,
653 London. pp407–420, 1966.
654
- 655 Kelaher, B.P.: Influence of physical characteristics of coralline turf on associated
656 macrofaunal assemblages, *Mar. Ecol. Prog. Ser.*, 232, 141–148, 2002.
657
- 658 Kelaher, B.P.: Changes in habitat complexity negatively affect diverse gastropod
659 assemblages in coralline algal turf, *Oecologia*, 135, 431–441, 2003.
660
- 661 Koch, M., Bowes, G., Ross, C. and Zhang, X-H.: Climate change and ocean
662 acidification effects on seagrasses and marine macroalgae, *Glob. Chang. Biol.*, 19, 103–
663 32, 2013.
664
- 665 Lee, D. and Carpenter, S.J.: Isotopic disequilibrium in marine calcareous algae, *Chem.*
666 *Geol.*, 172, 307–329, 2001.
667
- 668 Littler, M.: Calcification and its role among the macroalgae, *Micronesica*, 12(1), 27–
669 41, 1976.
670
- 671 Littler, M., Littler, D.S., Blair, S.M. and Norris, J.N.: Deepest known plant life
672 discovered on an uncharted seamount, *Science*, 227, 57–59, 1985.
673
- 674 Lüning, K.: *Seaweeds: their environment, biogeography and ecophysiology*, John
675 Wiley & Sons, New York, NY, USA, 1990.
676
- 677 Martin, S., Castets, M.D. and Clavier, J.: Primary production, respiration and
678 calcification of the temperate free-living coralline alga *Lithothamnion corallioides*,
679 *Aquat. Bot.*, 85, 121–128, 2006.



- 680 Martin, S., Clavier, J., Chauvaud, L. and Thouzeau, G.: Community metabolism in
681 temperate maerl beds. I. Carbon and carbonate fluxes, *Mar. Ecol. Prog. Ser.*, 335, 19–
682 29, 2007.
- 683
684 Martin, S. and Gattuso, J-P.: Response of Mediterranean coralline algae to ocean
685 acidification and elevated temperature, *Glob. Chang. Biol.*, 15, 2089–2100, 2009.
- 686
687 McCoy, S. and Kamenos, N.A.: Coralline algae (Rhodophyta) in a changing world:
688 integrating ecological, physiological, and geochemical responses to global change, *J.*
689 *Phycol.*, DOI: 10.1111/jpy.12262, 2015.
- 690
691 Mehrbach, C., Culberson, C.H., Hawley, J.E. and Pytkowicz, R.M.: Measurement of
692 the apparent dissociation constants of carbonic acid in seawater at atmospheric
693 pressure, *Limnol. Oceanogr.*, 18, 897–907, 1973.
- 694
695 Millero, F.J.: The marine inorganic carbon cycle, *Chem. Rev.*, 107, 308–341, 2007.
- 696
697 Morris, S. and Taylor, A.C.: Diurnal and seasonal-variation in physicochemical
698 conditions within intertidal rock pools, *Estuar. Coast Shelf Sci.*, 17, 339–355, 1983.
- 699
700 Nelson, W.A.: Calcified macroalgae - critical to coastal ecosystems and vulnerable to
701 change: a review, *Mar. Freshw. Res.*, 60, 787, 2009.
- 702
703 Perkins, R.G., Williamson, C.J., Brodie, J., Barille, L., Launeau, P., Lavaud, J., Yallop,
704 M.L. and Jesus, B.: Microspatial variability in community structure and
705 photophysiology of calcified macroalgal microbiomes revealed by coupling of
706 hyperspectral and high-resolution fluorescence imaging, *Scientific Reports*, 6, 22343,
707 2016.
- 708
709 Pentecost, A.: Calcification and photosynthesis in *Corallina officinalis* L. using CO₂-
710 14 method, *Br. Phycol. J.*, 13, 383–390, 1978.
- 711
712 Pierrot, D., Lewis, E. and Wallace, D.W.R.: MS Excel program developed for CO₂
713 system calculations, Tech. rep., Carbon Dioxide Inf. Anal. Cent., Oak Ridge Natl. Lab,
714 US DOE, Oak Ridge, Tennessee, 2016.
- 715
716 R Core Team: R: A Language and Environment for Statistical Computing, 2014.
- 717
718 Ries, J.B.: Effects of secular variation in seawater Mg/Ca ratio (calcite-aragonite seas)
719 on CaCO₃ sediment production by the calcareous algae *Halimeda*, *Penicillus* and
720 *Udotea* - evidence from recent experiments and the geological record, *Terra. Nov.*, 21,
721 323–339, 2009.
- 722
723 Smith, S. and Key, G.: Carbon dioxide and metabolism in marine environments,
724 *Limnol. Oceanogr.*, 20, 493–495, 1975.
- 725
726 Van der Heijden, L.H. and Kamenos, N.A.: Calculating the global contribution of
727 coralline algae to total carbon burial, *Biogeosciences*, 12, 6429–6441, 2015.
- 728



729 Venables, W.N. and Ripley, B.D.: Modern Applied Statistics with S, Fourth. Springer,
730 New York, 2002.

731

732 Williamson, C.J., Brodie, J., Goss, B., Yallop, M., Lee, S. and Perkins, R.: *Corallina*
733 and *Ellisolandia* (Corallinales, Rhodophyta) photophysiology over daylight tidal
734 emersion: interactions with irradiance, temperature and carbonate chemistry, *Mar.*
735 *Biol.*, 161, 2051–2068, 2014a.

736

737 Williamson, C.J., Najorka, J., Perkins, R., Yallop, M.L. and Brodie, J.: Skeletal
738 mineralogy of geniculate corallines: providing context for climate change and ocean
739 acidification research, *Mar. Ecol. Prog. Ser.*, 513, 71–84, 2014b.

740

741 Williamson, C.J., Walker, R.H., Robba, L., Russell, S., Irvine, L.M. and Brodie, J.:
742 Towards resolution of species diversity and distribution in the calcified red algal genera
743 *Corallina* and *Ellisolandia* (Corallinales, Rhodophyta), *Phycologia*, 54(1), 2–11, 2015.

744

745 Zou, D., Kunshan, G.A.O. and Jianrong, X.I.A.: Dark respiration in the light and in
746 darkness of three marine macroalgal species grown under ambient and elevated CO₂
747 concentrations, *Acta. Oceanol. Sin.*, 30(1), 106–112, 2011.

748

749

750

751

Figures



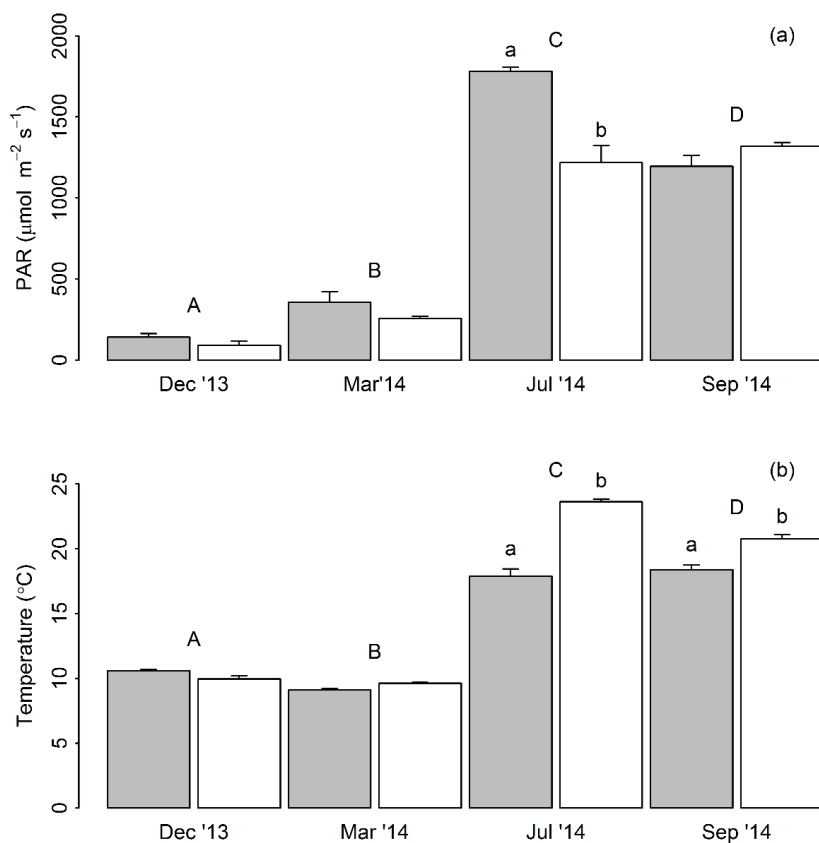
752

753 **Figure 1.** Sampling site and habitat, showing location of Combe Martin (a), and an

754 example upper-shore rock pool (b) dominated by turfing assemblages of *Corallina*

755 *officinalis* (c).

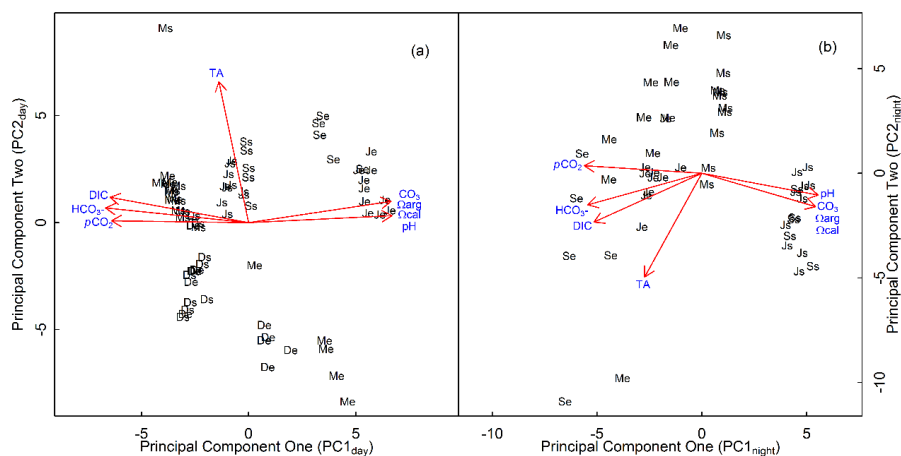
756



757

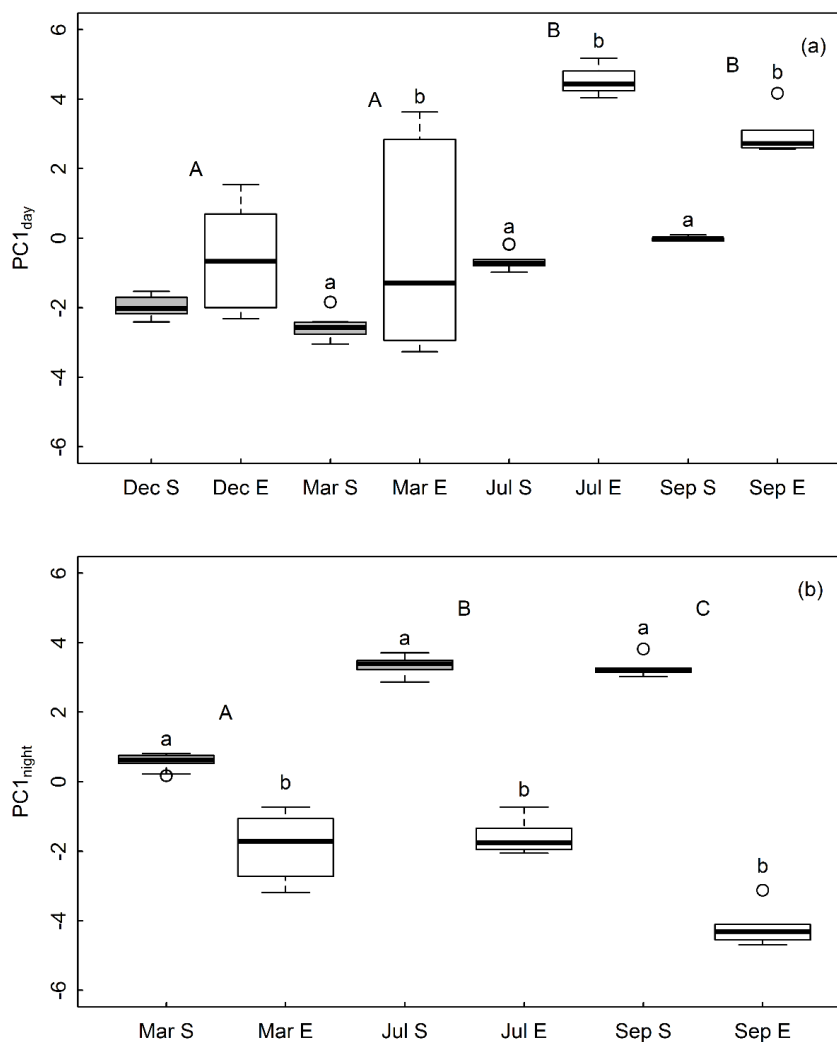
758 **Figure 2:** Irradiance (a) and rock pool water temperature (b) recorded at the start (grey
759 bars) and end (white bars) of daytime tidal emersion periods during December 2013
760 (Dec '13), and March (Mar '14), July (Jul'14) and September (Sep '14) 2014 (Average
761 \pm SE). Upper-case and lower-case letters denote TukeyHSD homogenous subsets in
762 relation to the factors 'month' and 'tide', respectively.

763



764
765 **Figure 3:** Principal components analysis of (a) daytime and (b) night-time carbonate
766 chemistry parameters, showing principal component one in relation to principal
767 component two. Upper-case letters indicate sampling month (D = December, M =
768 March, J = July, S = September) and lower-case letters indicate start (s) or end (e) tidal
769 emersion.

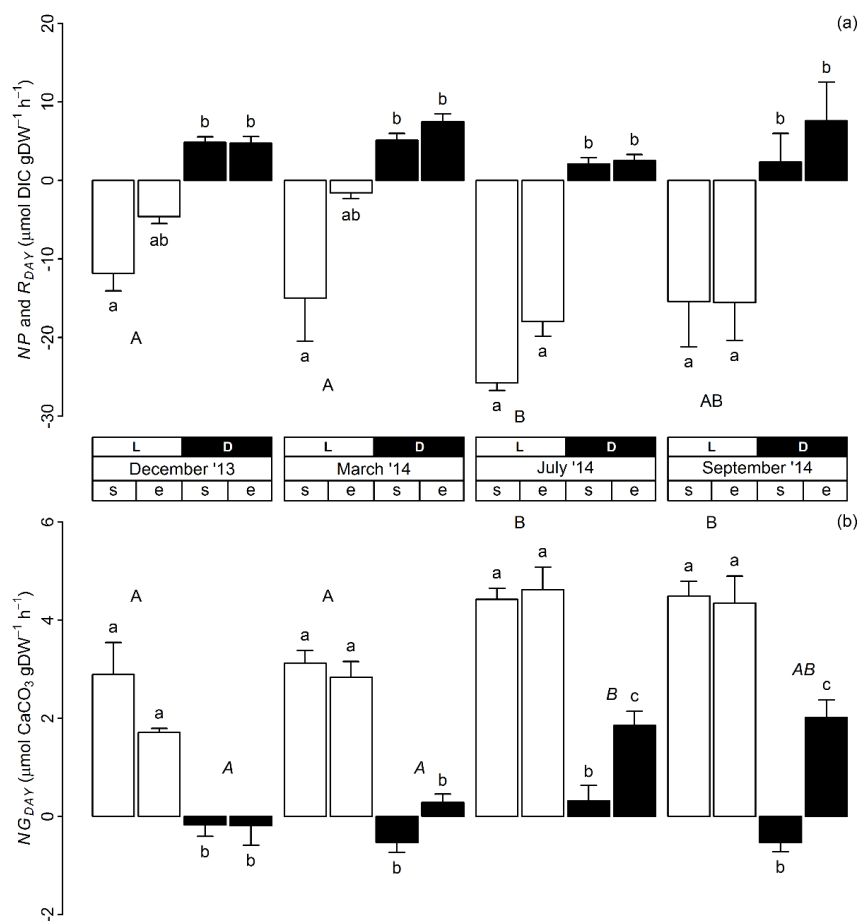
770



771

772 **Figure 4:** Boxplots showing the median, minimum, maximum and first and third
 773 quartiles of PC1_{day} (a) and PC1_{night} (b) in relation to sampling month (Dec = December,
 774 Mar = March, Jul = July, Sep = September) and tidal emersion period (S = start, E =
 775 End). Upper-case and lower-case letters denote TukeyHSD homogenous subsets in
 776 relation to the factors ‘month’ and ‘tide’, respectively.

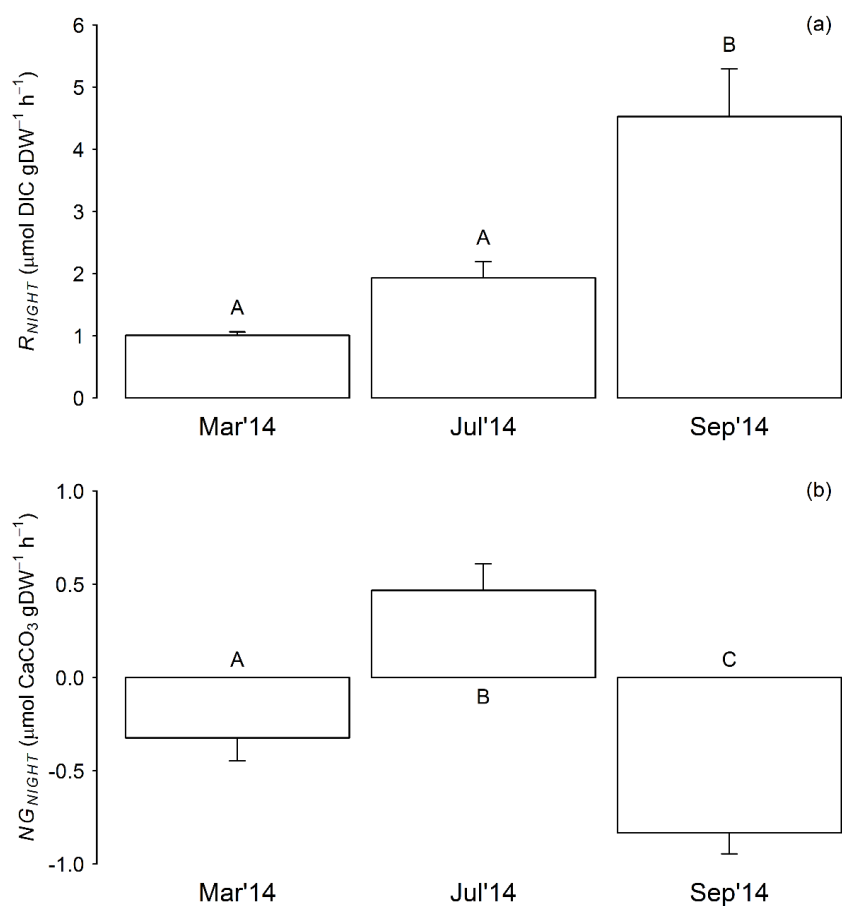
777



778

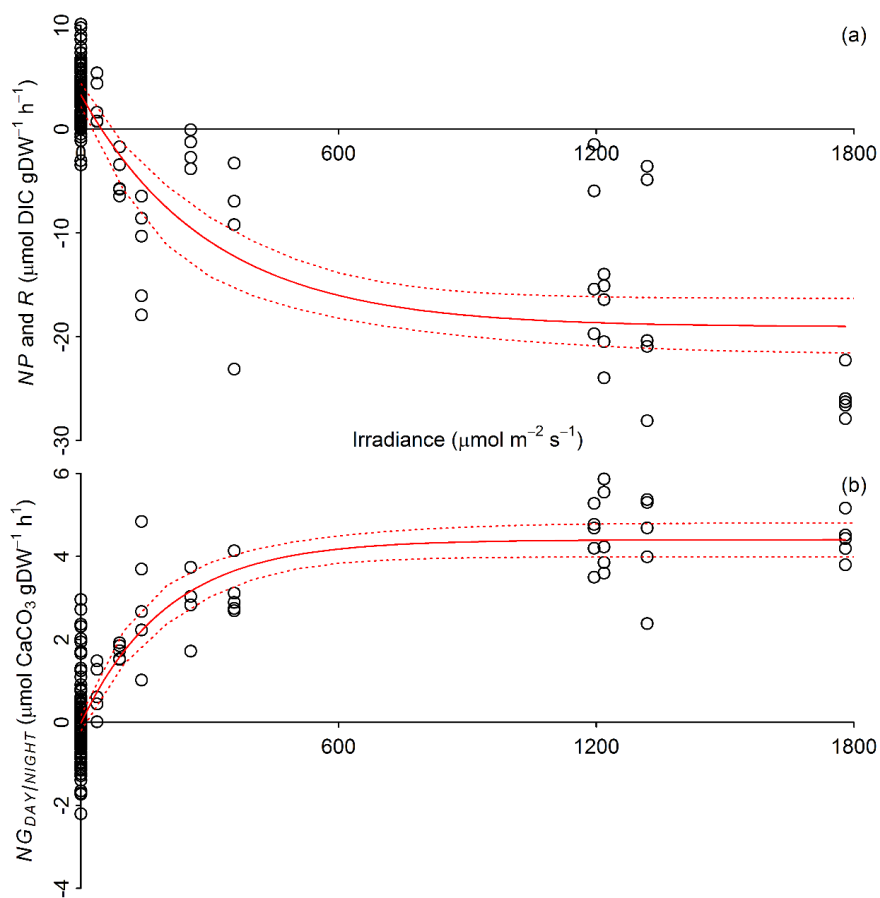
779 **Figure 5:** Average daytime (a) NP (-ve DIC flux) and R_{DAY} (+ve DIC flux), and (b)
 780 N_{GDAY} as determined from light (L – white bars) and dark (D – black bars) treatment
 781 incubations conducted at the start (s) and end (e) of daytime tidal emersion periods
 782 during December 2013 and March, July and September 2014 (Average \pm SE, $n = 5$).
 783 Upper-case and lower-case letters denote TukeyHSD homogenous subsets in relation
 784 to the factors ‘month’ and ‘tide’, respectively.

785



786
787 **Figure 6:** Average night-time (a) R_{NIGHT} and (b) NG_{NIGHT} as determined across both
788 light/dark treatment incubations and the start/end of tidal emersion periods (Average
789 \pm SE, $n = 20$). Upper-case letters denote TukeyHSD homogenous subsets in relation
790 to the factor 'month'.

791

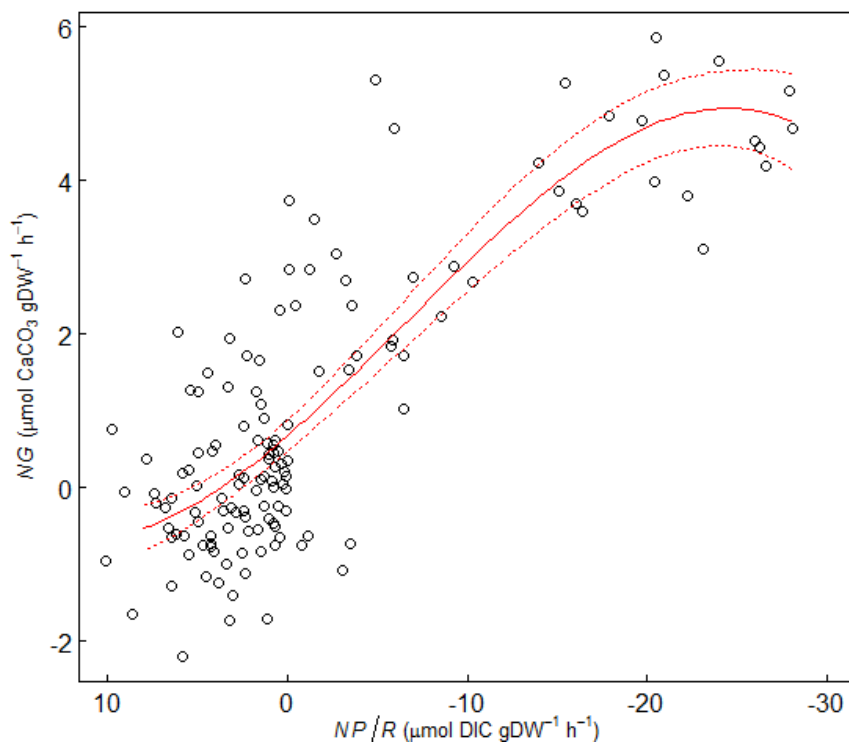


792

793 **Figure 7:** Relationship of (a) net production/respiration (NP and R) and (b) net
 794 calcification ($NG_{DAY/NIGHT}$) with irradiance (Model 1, Table 4), showing regression line
 795 (solid red line) and 95 % confidence intervals (dashed red lines).

796

797



798
799

800 **Figure 8:** Relationship between calcification (NG) and production / respiration (NP/R),
801 showing regression line (solid red line) and 95 % confidence intervals (dashed red
802 lines).

803
804
805
806
807
808
809
810
811
812
813



814

Tables

815

816 **Table 1:** Sampling dates and tidal details. All times are expressed in GMT.

Sampling Date							
Dec 4 th /5 th 2013		Mar 16 th /17 th 2014		Jul 1 st /2 nd 2014		Sep 9 th /10 th 2014	
Time	Height (m)	Time	Height (m)	Time	Height (m)	Time	Height (m)
06:30	9.6	05:50	8.8	08:12	8.4	05:46	9.7
12:30	0.7	11:51	1.2	13:59	1.6	11:50	0.4
18:50	9.5	18:09	8.9	20:23	8.5	18:08	10.1
00:55	0.8	00:02	1	02:20	1.7	00:13	0.2
07:15	9.7	06:23	9	08:45	8.2	06:31	9.9

817

818

819 **Table 2:** Component loadings of principal components analysis of daytime and night-820 time carbonate chemistry parameters (TA, DIC, pH, $p\text{CO}_2$, HCO_3^- , CO_3^{2-} , Ω_{arg} and Ω_{cal})

821

	PC1 _{DAY} (%)	PC2 _{DAY} (%)	PC1 _{NIGHT} (%)	PC2 _{NIGHT} (%)
Proportion of variance	84.3	13.2	83.6	16.0
Cumulative proportion	84.3	97.6	83.6	99.7
Variable	PC1 _{DAY}	PC2 _{DAY}	PC1 _{NIGHT}	PC2 _{NIGHT}
Component Loadings				
TA	-0.07	0.94	-0.18	-0.77
DIC	-0.36	0.17	-0.35	-0.36
pH	0.38	0.04	0.37	-0.16
$p\text{CO}_2$	-0.36	0.01	-0.38	0.05
HCO_3^-	-0.38	0.09	-0.37	-0.23
CO_3^{2-}	0.37	0.14	0.37	-0.24
Ω_{arg}	0.37	0.14	0.37	-0.24
Ω_{cal}	0.37	0.14	0.37	-0.24

822



Table 3: Multiple linear regression analysis of PCI_{DAY} in relation to irradiance (Irrad.) or cumulative photodose (Photo.) plus water temperature (Temp.), and linear regression analysis of PCI_{NIGHT} in relation to water temperature (Temp.), showing associated standard error (SE) of coefficients, the significance of predictor variables (Pred. sig.) within the model, the percent relative importance of predictor variables (Rel. Imp.), the proportion of variance explained by the regression (R^2), the overall model significance (P), and the number of observations (n).

Relationship ($y = a + b_1 * X_1 + b_2 * X_2$)	Coefficient SE		Pred. sig.		Rel. Imp. (%)		R^2	P	n	
	a	b_1	b_2	X_1	X_2	X_1				X_2
$PCI_{DAY} = -7.03 + -0.002 * Irrad. + 0.61 * Temp.$	0.73	0.00	0.07	<0.001	<0.001	28	71	0.63	<0.001	96
$PCI_{DAY} = -2.52 + 1.41^{*7} * Photo. + 9.10^{-2} * Temp.$	0.72	2.72 ^s	6.38 ^{s2}	<0.001	<0.01	58	41	0.69	<0.001	96
$PCI_{NIGHT} = -2.89 + 0.22 * Temp.$	1.40	0.10	-	<0.05	<0.05	-	-	0.08	<0.05	72



- 1 **Table 4:** Values of parameters (*SE* in parentheses) calculated by non-linear regression of net production (*NP*, $\mu\text{mol DIC gDW}^{-1} \text{h}^{-1}$) and net
 2 calcification (*NG*, $\mu\text{mol CaCO}_3 \text{gDW}^{-1} \text{h}^{-1}$): in relation to (Model 1) irradiance (*E*, $\mu\text{mol photons m}^{-2} \text{s}^{-1}$), where *c* is estimated dark respiration or
 3 calcification; and in relation to (Model 2) irradiance and temperature (*T*, °C), where *f* is a constant; and in relation to (Model 3) irradiance and
 4 carbonate chemistry (*PCI*); and in relation to (Model 4) irradiance, temperature and carbonate chemistry. Asterisks denote coefficient significance
 5 in models ($P < 0.05^*$, $P < 0.01^{**}$, $P < 0.001^{***}$). Estimation of overall model fit is presented as the proportion of variance explained by the
 6 regression (R^2) and as Akaike Information Criterion (*AIC*). *n* denotes the number of observations.

	$P(G)_{max}$	E_k	<i>c</i>	<i>d</i>	<i>e</i>	<i>f</i>	R^2	<i>AIC</i>	<i>n</i>
Model 1: $NP(NG) = P(G)_{max}(1 - e^{-E/E_k}) + c$									
<i>NP</i>	-22.3(1.48)***	300(65)***	3.29(0.56)***				0.67	885	140
<i>NG</i>	4.41(0.22)***	200(34)***	-0.01(0.09)**				0.76	383	140
Model 2: $NP(NG) = P(G)_{max}(1 - e^{-E/E_k}) + dT + f$									
<i>NP</i>	-23.8(1.97)***	377(99)***		0.15(0.12)		1.07(1.82)	0.68	886	140
<i>NG</i>	3.92(0.21)***	115(24)***		0.08(0.01)***		-1.28(0.26)***	0.80	363	140
Model 3: $NP(NG) = P(G)_{max}(1 - e^{-E/E_k}) + ePCI + f$									
<i>NP</i>	-23.0(1.62)***	343(80)***			0.29(0.20)	3.24(0.56)***	0.68	885	140
<i>NG</i>	4.18(0.21)***	149(27)***			0.13(0.03)***	-0.03(0.08)*	0.79	367	140
Model 4: $NP(NG) = P(G)_{max}(1 - e^{-E/E_k}) + dT + ePCI + f$									
<i>NP</i>	-23.6(1.96)***	375(99)***		0.07(0.14)	0.22(0.23)	2.12(2.12)	0.68	887	140
<i>NG</i>	3.94(0.20)***	113(23)***		0.06(0.02)**	0.08(0.03)*	-0.93(0.30)**	0.80	360	140